

ORIGINAL RESEARCH

The RNA Polymerase III Subunit Polr3b Is Required for the Maintenance of Small Intestinal Crypts in Mice

Julia E. Kieckhaefer,^{1,2,§} Sabina Lukovac,^{1,2,§} Diana Z. Ye,^{1,2} Dolim Lee,^{1,2} Danielle J. Beetler,¹ Michael Pack,³ and Klaus H. Kaestner^{1,2}¹Department of Genetics, ²Institute for Diabetes, Obesity, and Metabolism, ³Department of Cell and Developmental Biology, University of Pennsylvania, Perelman School of Medicine, Philadelphia, Pennsylvania

SUMMARY

RNA polymerase III activity is increased in some cancers. Effects of its inhibition in mammals are not known. We show that a mutation in the Pol III subunit Polr3b in the murine intestine results in crypt failure and increased mortality. Our conditional model will allow for the study of Polr3b function in all cell types in the mouse.

BACKGROUND & AIMS: The continuously self-renewing mammalian intestinal epithelium, with high cellular turnover, depends on adequate protein synthesis for its proliferative capacity. RNA polymerase III activity is related closely to cellular growth and proliferation. Here, we studied the role of Polr3b, a large RNA polymerase III subunit, in the mammalian intestinal epithelium.

METHODS: We derived mice with an intestinal epithelium-specific hypomorphic mutation of the *Polr3b* gene, using VillinCre-mediated gene ablation. Phenotypic consequences of the *Polr3b* mutation on the intestinal epithelium in mice were assessed using histologic and molecular methodologies, including genetic lineage tracing.

RESULTS: The *Polr3b* mutation severely reduced survival and growth in mice during the first postnatal week, the period when the expansion of the intestinal epithelium, and thus the requirement for protein synthesis, are highest. The neonatal intestinal epithelium of *Polr3b*^{loxP/loxP};VillinCre mice was characterized by areas with reduced proliferation, abnormal epithelial architecture, loss of Wnt signaling, and a dramatic increase in apoptotic cells in crypts. Genetic lineage tracing using *Polr3b*^{loxP/LoxP};Rosa26-lox-stop-lox-YFP;VillinCre mice showed that in surviving mutant mice, Polr3b-deficient dying crypts were replaced progressively by Cre-escaper cells that had retained wild-type Polr3b function. In addition, enteroids cultured from *Polr3b*^{loxP/loxP};VillinCre mice showed reduced proliferative activity and increased apoptosis.

CONCLUSIONS: We provide evidence for an essential role of the RNA polymerase III subunit Polr3b in orchestrating the maintenance of the intestinal crypt during early postnatal development in mice. (*Cell Mol Gastroenterol Hepatol* 2016;2:783–795; <http://dx.doi.org/10.1016/j.jcmgh.2016.08.003>)

Keywords: Polr3b; Pol III; Intestinal Epithelium; Crypts; Enteroids.

The small intestinal epithelium is the fastest self-renewing tissue in mammals, and thus highly dependent on adequate protein synthesis for proliferation, especially during early postnatal development, when the expansion of the epithelial layer takes place. In neonatal mice, intervillus regions of the intestinal epithelium reorganize to give rise to highly proliferative crypt structures, which increase in number and size during this transition from neonatal to adult function.¹

The RNA polymerase III (Pol III) complex transcribes small noncoding RNAs (sncRNAs), such as transfer RNAs (tRNAs), U6 snRNAs, and 5S ribosomal RNAs (rRNAs),² which all are involved directly or indirectly in protein synthesis. Studies in *Saccharomyces cerevisiae* have shown many factors and mechanisms that regulate Pol III transcription.³ These studies clearly show that high Pol III activity is required during conditions of rapid growth, whereas reduction in Pol III activity is observed during nutrient deprivation.⁴ Although the Pol III complex is highly conserved from yeast to human beings, unlike in yeast, Pol III targets are repressed differentially in response to nutrient deprivation in human fibroblasts, indicating that mechanisms of transcriptional regulation of Pol III genes are more complex in mammals.⁵

Although Pol III traditionally has been regarded as functioning in a housekeeping capacity, studies in metazoans have shown sophisticated mechanisms of transcriptional regulation of Pol III targets, including cell type-specific transcription of different tRNA genes.⁶ In mammalian cells, numerous studies have pointed to Pol III dysregulation as playing a role in oncogenic transformation.^{6,7} In support of this finding, overexpression of Pol III transcripts has been described in multiple cancers

[§]Authors share co-senior authorship.

Abbreviations used in this paper: cDNA, complementary DNA; E, embryonic day; PCR, polymerase chain reaction; Pol III, polymerase III; qPCR, quantitative polymerase chain reaction; rRNA, ribosomal RNA; slj, slim jim; snoRNA, small nucleolar RNA; snRNA, small non-coding RNA; tRNA, transfer RNA; TUNEL, terminal deoxynucleotidyl transferase-mediated deoxyuridine triphosphate nick-end labeling.

Most current article

© 2016 The Authors. Published by Elsevier Inc. on behalf of the AGA Institute. This is an open access article under the CC BY-NC-ND license (<http://creativecommons.org/licenses/by-nc-nd/4.0/>).
2352-345X

<http://dx.doi.org/10.1016/j.jcmgh.2016.08.003>

and in transformed cell lines.^{8–11} The proto-oncogene proteins mechanistic target of rapamycin complex 1 (mTORC1), myelocytomatosis oncogene (MYC), p53, and retinoblastoma all directly regulate transcription by Pol III in human cells.^{12–15} Thus, comprehending the function and regulation of Pol III is vital to the understanding of tissue growth in health and disease.

Despite the importance of Pol III, little is known about its requirement during development. In zebrafish, a large-scale mutagenesis screen recovered a mutation, termed *slim jim* (*slj*), that causes an in-frame deletion in the gene encoding the second-largest Pol III subunit, *Polr3b*.¹⁶ The mutation has a profound effect on the proliferation and growth of intestinal epithelial progenitor cells, consistent with a high demand for protein synthesis in the rapidly proliferating intestinal epithelium.

The continuously self-renewing mammalian intestinal epithelium, with high cellular turnover, provides an attractive system to study the role of the Pol III complex in mammalian cell proliferation. Based on data from previous studies in the *slj* zebrafish, we hypothesized that *Polr3b* might play an important role in the growth and development of the mammalian gut. To study this hypothesis, we generated a conditional hypomorphic mutation of *Polr3b* specifically in the mouse intestinal epithelium.

Here, we show that the disruption of the Pol III complex in the intestinal epithelium by *Polr3b* mutation leads to a severe developmental phenotype, mainly characterized by increased mortality, accompanied by reduced proliferative and differentiation capacity, impaired crypt maturation, and reduced Wnt signaling in the intestinal epithelium. In summary, our data show the important role of RNA polymerase III in regulating the establishment of the intestinal epithelium in mammals.

Methods

Derivation of *Polr3b*^{loxP/loxP}; *VillinCre* Mice

The *Polr3b* conditional mutant allele was derived in mouse embryonic stem cells via homologous recombination using the targeting construct shown in Figure 1A. LoxP sites flanking exon 10 allow for ablation of exon 10 in *Polr3b*^{loxP/loxP} upon Cre activation. The neomycin cassette was excised by crossing the F1 offspring with *Flp1* deleter mice.¹⁷ To ablate *Polr3b* conditionally in the intestinal epithelium, *Polr3b*^{loxP/+} mice were crossed with *VillinCre* mice, kindly provided to us by Deborah Gumucio,¹⁸ to obtain *Polr3b*^{loxP/+}; *VillinCre* and *Polr3b*^{loxP/loxP}; *VillinCre* mice. Genotyping was performed by polymerase chain reaction (PCR) analysis of genomic tail DNA (data not shown). The following primers were used to detect the *Polr3b* wild-type and mutant allele, yielding a 222-bp product and a 519 bp product, respectively: 5'-AGCCTCATTTCTTCGTGGTGA-3' and 5'-TGGCCTAGGAAGGAAGAAAA-3'. *Polr3b*^{loxP/+}; *VillinCre* and *Polr3b*^{loxP/loxP} mice show no abnormalities and are viable and fertile. The Cre transgene was detected using: 5'-GCGGCATGGTGAAGTTGAAT-3' and 5'-CGTTCACCGGCATCAACGTTT-3' primers (product size, 232 bp). To perform lineage tracing experiments, *Polr3b*^{loxP/+}; *VillinCre* and

Polr3b^{loxP/loxP} mice were crossed with *R26-stop-EYFP* mice (*B6.129X1-Gt[ROSA]26Sor^{tm1(EYFP)Cos}/J*) obtained from The Jackson Laboratory (Bar Harbor, ME). All procedures involving mice were conducted in accordance with approved Institutional Animal Care and Use Committee protocols.

Laser Capture Microdissection and Subsequent PCR Analysis of Wild-Type and Mutant Alleles

Paraffin-fixed intestinal tissue was sectioned (5 μm) on nuclease and nucleic acid-free frame slides for laser microdissection (Part #: FS-LMD-M-50r; MicroDissect GmbH; Herborn, Germany). Unstained and dehydrated tissue was air-dried and processed immediately for laser capture microdissection. Crypt regions were dissected from *Polr3b*^{loxP/loxP}; *VillinCre* mice and their wild-type littermates into PCR sample tubes for laser microdissection (ASSEE, ST-LMD-M-500), subsequent overnight proteinase K digestion, and PCR analysis for the presence of the wild-type and mutant *Polr3b* allele using the following primers: 5'-GACGAATTCCTGCAGCCCAAT-3' (*Polr3bF*) with 5'-CCCTGGAAATGAACAGGGGAAA-3' (*Polr3bR1*), which yields a wild-type product of 930 bp and a mutant product of 337 bp. Additional PCR analysis was performed using the same *Polr3bF* primer and the *Polr3bR2* primer: 5'-GTGGCCGCTTACTGATGAA-3' to detect only the wild-type product of 530 bp.

Antibodies

The following antibodies were used for immunofluorescent or immunohistochemical analysis: rabbit anti-Ki67 (VP-K451, 1:1000; Vector Laboratories; Burlingame, CA), rabbit anti-lysozyme (A0099, 1:1000; Dako; Glostrup Municipality, Denmark), mouse anti-E-cadherin (610181, 1:500; BD Transduction Laboratories; San Jose, CA), chicken anti-green fluorescent protein (GFP) for the detection of enhanced yellow fluorescent protein (EYFP) (GFP-1020, 1:2000; Aves Labs; Tigard, OR), rabbit anti-cyclin D1 (CRM 307, 1:100; Biocare Medical; Concord, CA), rabbit anti-cleaved caspase-3 (9661, 1:200; Cell Signaling Technology; Danvers, MA), mouse anti-β-catenin (610153, 1:200; BD Biosciences, San Jose, CA), and rabbit anti-mucin 2 (sc-15334, 1:1000; Santa Cruz Biotechnology; Dallas, TX). Cy2- and Cy3-conjugated fluorescent secondary antibodies were purchased from The Jackson Laboratory and used at a 1:200 dilution. Biotinylated secondary antibodies for immunohistochemical assays (Vector Laboratories) were used at a 1:200 dilution along with the ABC detection system (PK-6100; Vector Laboratories).

Terminal Deoxynucleotidyl Transferase-Mediated Deoxyuridine Triphosphate Nick-End Labeling Assay

To detect apoptotic cells in the intestinal epithelium, we performed the terminal deoxynucleotidyl transferase-mediated deoxyuridine triphosphate nick-end labeling (TUNEL) assay using an in situ cell death detection kit according to the manufacturer's instructions (Roche Applied Science; Penzberg, Germany). Cell death was

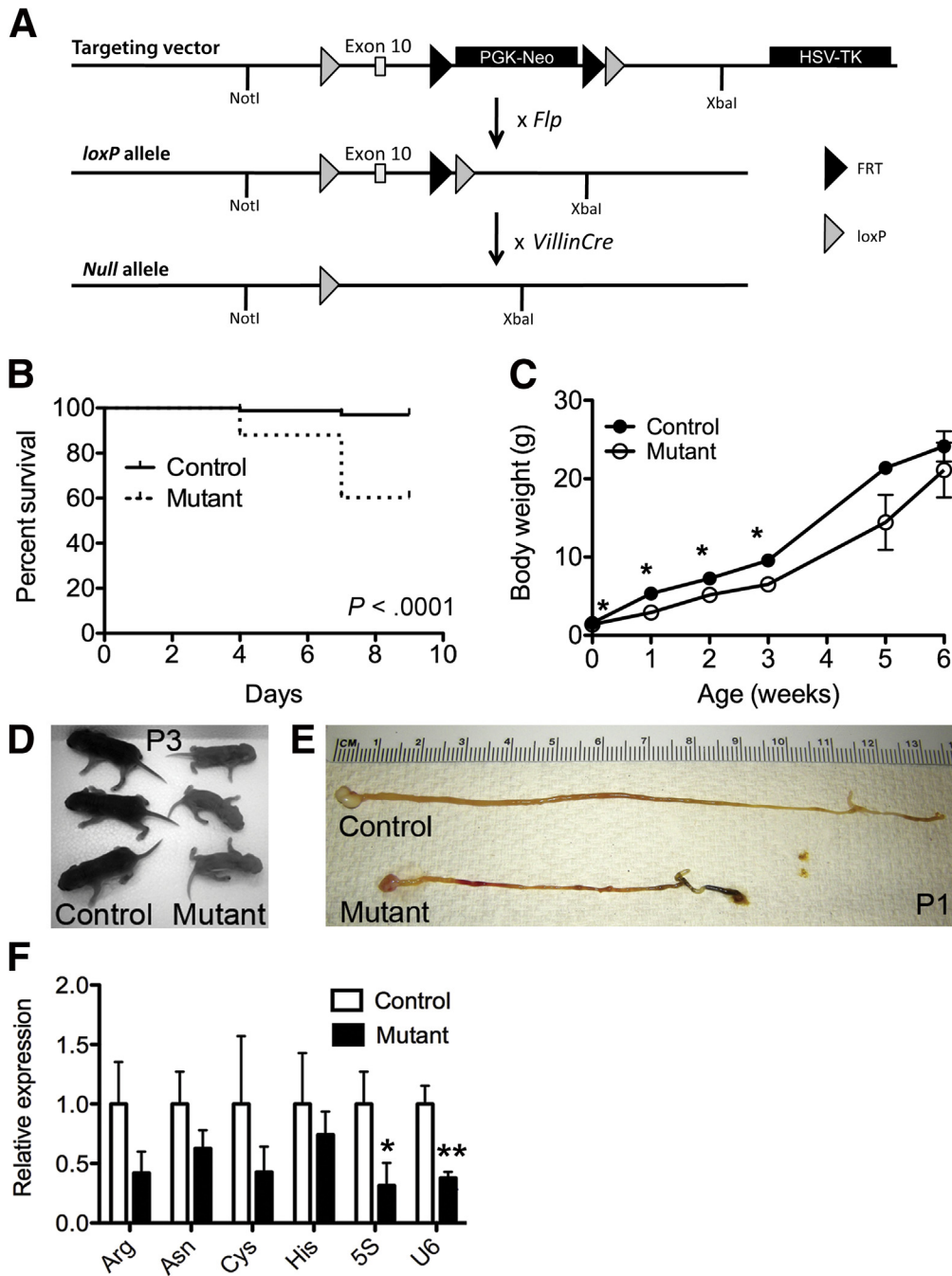


Figure 1. Intestine-specific, conditional hypomorphic mutation of the *Polr3b* gene, encoding a large subunit of RNA polymerase III, causes reduced survival, delayed growth, and decreased intestinal epithelial transcription of snRNAs. (A) Targeting strategy used for conditional ablation of exon 10 of the *Polr3b* gene. After germ-line transmission, the FRT-flanked neomycin resistance gene (PGK-Neo cassette) was excised by crossing to *Flp* deleter mice (*Flp*). *Polr3b*^{loxP/loxP}; *VillinCre* mice were derived by intercrossing *Polr3b*^{loxP/+} with *VillinCre* mice. (B) Kaplan–Meier survival curve of control and mutant mice during the first 8 postnatal days, showing a significantly lower survival rate in *Polr3b*-mutant mice compared with littermate controls (log-rank [Mantel–Cox] and Gehan–Breslow–Wilcoxon test; *P* < .0001, *N* = 12–28). (C) Significantly reduced body weight during the preweaning period in *Polr3b*-mutant mice (means ± SEM; **P* < .05; *N* = 3–47). During weaning, when the regenerative response was observed, *Polr3b*-mutant mice started to catch up in body weight with their littermate controls. (D) *Polr3b*-mutant mice (right) are visibly smaller than their control littermates (left), on postnatal day 3 (P3). (E) P1 control and mutant stomach, large intestine, and colon. (F) Real-time qPCR analysis of expression of tRNA-Arg, tRNA-Asn, tRNA-Cys, tRNA-His, 5S rRNA, and U6 snRNA in the jejunum of E18.5 control (*N* = 7) and mutant (*N* = 10) mice (means ± SEM; **P* = .0496, Student *t* test; ***P* = .002, Mann–Whitney test). Data were normalized to the means of snoRNA 202 and snoRNA 234.

quantified by counting the number of TUNEL-positive cells per crypt in jejunal sections from P21 mice (control, N = 4; mutant, N = 4). An average of 20 crypts were counted per animal.

Quantitative PCR Analysis

For the analysis of stem cell markers, total RNA was extracted from the jejunal tissue using the TRIzol reagent method (15596-026; Invitrogen, Carlsbad, CA). Complementary DNA (cDNA) synthesis and quantitative PCR analysis were performed as described.¹⁹ Gene expression was normalized to messenger RNA levels of glyceraldehyde-3-phosphate dehydrogenase. Primer sequences used for the quantitative PCR analysis have been reported previously.²⁰⁻²³

To measure the expression of Pol III targets, total RNA was extracted from the jejunal tissue at embryonic day 18.5 (E18.5) mice using the *mirVana* miRNA Isolation Kit (AM1560; Life Technologies, Carlsbad, CA). cDNA synthesis and quantitative PCR analysis were performed using custom TaqMan Small RNA Assays (4440418; Life Technologies) for tRNA-Arg, tRNA-Asn, tRNA-Cys, tRNA-His, and 5S rRNA. TaqMan MicroRNA Assays (4427975; Life Technologies) were used for cDNA synthesis and quantitative PCR analysis of U6 snRNA, small nucleolar (snoRNA) 202, and snoRNA 234. Gene expression was normalized to the mean level of snoRNA 202 and snoRNA 234. Primer sequences are available on request.

Intestinal Crypt/Enteroid Culture

Small intestine was harvested from P1 *Polr3b*-mutant and control mice. After a 30-minute EDTA (5 mmol/L) incubation, the intestinal crypts were filtered through a 70- μ m cell strainer. Crypts were plated suspended in Matrigel (356231; BD Biosciences) and cultured in advanced Dulbecco's modified Eagle medium/F-12 (12634010; Thermo Fisher Scientific, Waltham, MA) containing the Wnt agonist R-spondin1 (Protein Expression Facility, The Wistar Institute, Philadelphia, PA), murine epidermal growth factor (PMG8043; Life Technologies), murine Noggin (250-38; Peprotech, Rocky Hill, NJ), and the Gsk3 inhibitor CHIR99021 (1677-5; BioVision, Milpitas, CA) as reported previously.^{24,25} On days 2, 4, and 6, pooled enteroids were genotyped by quantitative PCR (qPCR) for the presence of the deleted allele using primers *Polr3bF* and *Polr3bR1*, as described earlier, and the undeleted allele using primers *Polr3bF2*: 5'-GCTTGATATCGAATTCGGAAG-3' and *Polr3bR*: 5'-CCTCTCTGGAACCTCAACCAA-3'. The quantity of genomic DNA present in qPCR reactions was normalized to genomic β -actin. In addition, proliferation and apoptosis were assessed in developing enteroids by immunofluorescent analysis of Ki67 and cleaved caspase-3, respectively, as described earlier.

Statistical Analysis

Values represent means \pm standard error of the mean for the indicated number of mice per group. Differences between groups were determined using an unpaired

Student *t* test (2-tailed), with a significance cut-off *P* value of less than .05, unless indicated otherwise. The percentages of the undeleted allele quantified in enteroids by qPCR at 3 different time points (2, 4, and 6 days in culture) were compared using the Kruskal-Wallis test, followed by the Dunn multiple comparison test. Analysis was performed with GraphPad Prism 5 software (GraphPad Software, Inc, La Jolla, CA).

Results

Polr3b^{loxP/loxP}; *VillinCre* Mice Have Reduced Survival and Growth

To study the contribution of the RNA polymerase III complex in the intestinal epithelium of mice, we derived mice with a conditional hypomorphic mutation of the *Polr3b* gene, which encodes Polr3b, a major subunit of Pol III (Figure 1A). The *Polr3b* mutation resulted in major mortality, with only 60% of *Polr3b*^{loxP/loxP}; *VillinCre* mice (hereafter referred to as *Polr3b*-mutants) surviving the first postnatal week (Figure 1B). Surviving mutant mice lagged behind their control littermates in growth until the third postnatal week (Figure 1B and C). Though there was no difference in intestinal length when normalized to body weight (data not shown), early postnatal mutant mice were significantly smaller and had shorter intestines than their littermate controls (Figure 1C-E). As expected, before birth (E18.5), the intestinal tissue of *Polr3b*^{loxP/loxP}; *VillinCre* mice already showed a significant reduction in the expression levels of the 5S and U6 RNAs, key components of the ribosome and splicing machinery, respectively, compared with control (*Polr3b*^{loxP/loxP}) mice (Figure 1F). Milk was present in the stomach of *Polr3b*-mutant mice from the first postnatal day until 3 weeks of age (data not shown), suggesting that *Polr3b*-mutant mice fed normally.

Newborn *Polr3b*-Mutant Mice Show Reduced Proliferation and Impaired Crypt Development

Given the slower growth rate of mutant animals and the significant reduction in the mutant epithelium of RNAs required for translation, we hypothesized that there were defects in proliferation in the mutant intestine. Therefore, we performed immunostaining for Ki67, a protein that marks the transit-amplifying cells of the intestinal epithelium. *Polr3b*^{loxP/loxP}; *VillinCre* intestine had clear regions lacking Ki67-positive cells at P7, P14, and P21 (Figure 2D, F, and H), which was indicative of reduced proliferative capacity in the intestinal epithelium of young *Polr3b*-mutant mice. In addition, P14 mutant intestinal epithelial areas with reduced numbers of Ki67-positive cells were lacking fully developed crypts, which normally are present by this stage in control mice (Figure 2E vs F). In regions lacking Ki67, crypts still were not present by P21 in *Polr3b*-mutant mice (Figure 2H). At P21, the areas with reduced numbers of Ki67-positive cells were surrounded by hyperproliferative regions that had increased numbers of Ki67-positive cells (Figure 2H), suggesting regenerative mechanisms were activated in regions with surviving crypts.

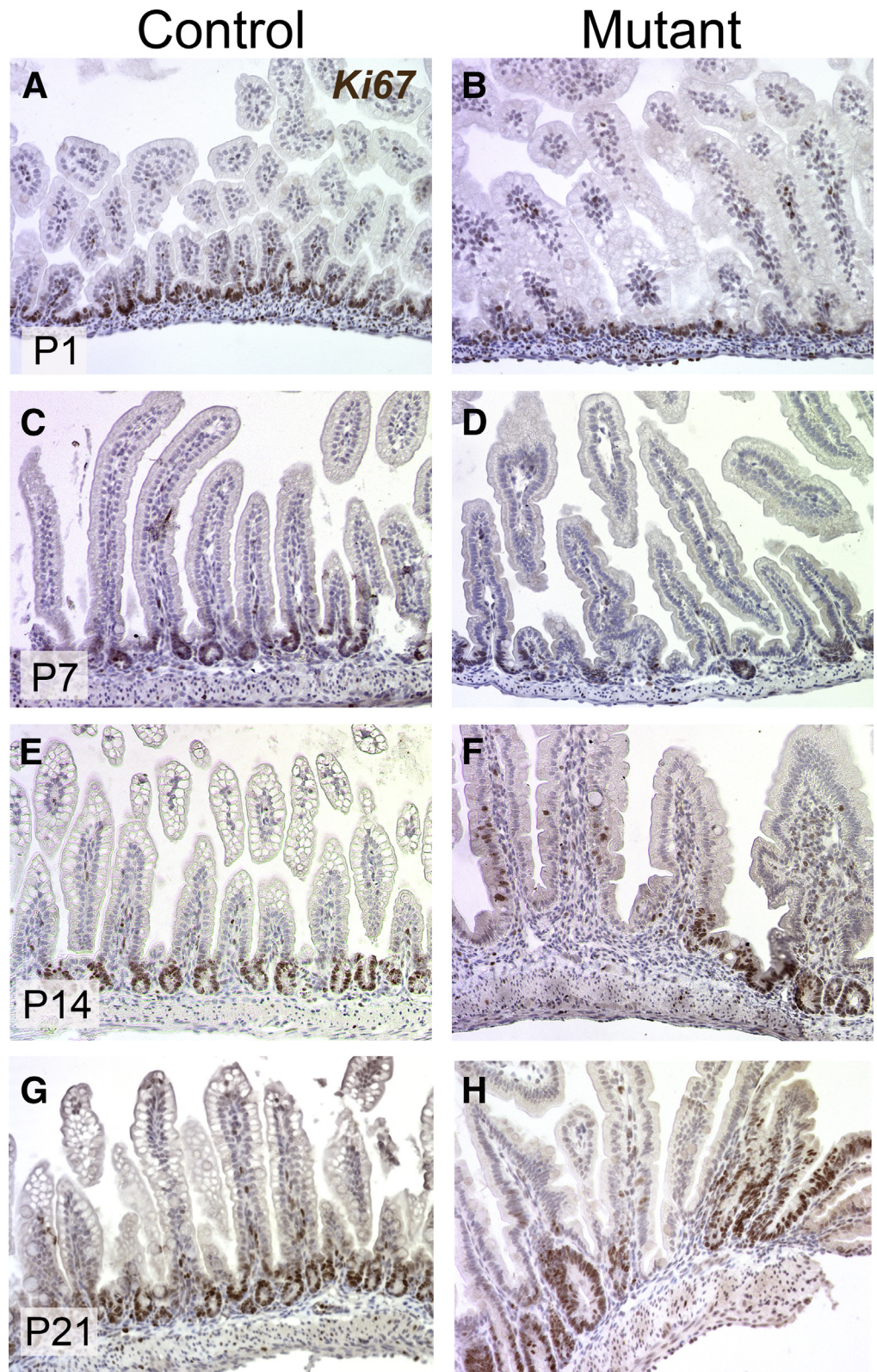


Figure 2. Proliferation is reduced in the small intestine of neonatal *Polr3b*^{loxP/loxP};*VillinCre*, followed by sporadic hyperplasia and enhanced proliferative activity during weaning. Ki67 immunohistochemistry of control and *Polr3b*-mutant mice at (A and B) P1, (C and D) P7, (E and F) P14, and (G and H) P21. At all stages, *Polr3b*-mutant mice show jejunal regions lacking Ki67-positive cells. At P21, the epithelium of *Polr3b*-mutant mice shows hyperproliferative regions with expanded crypts.

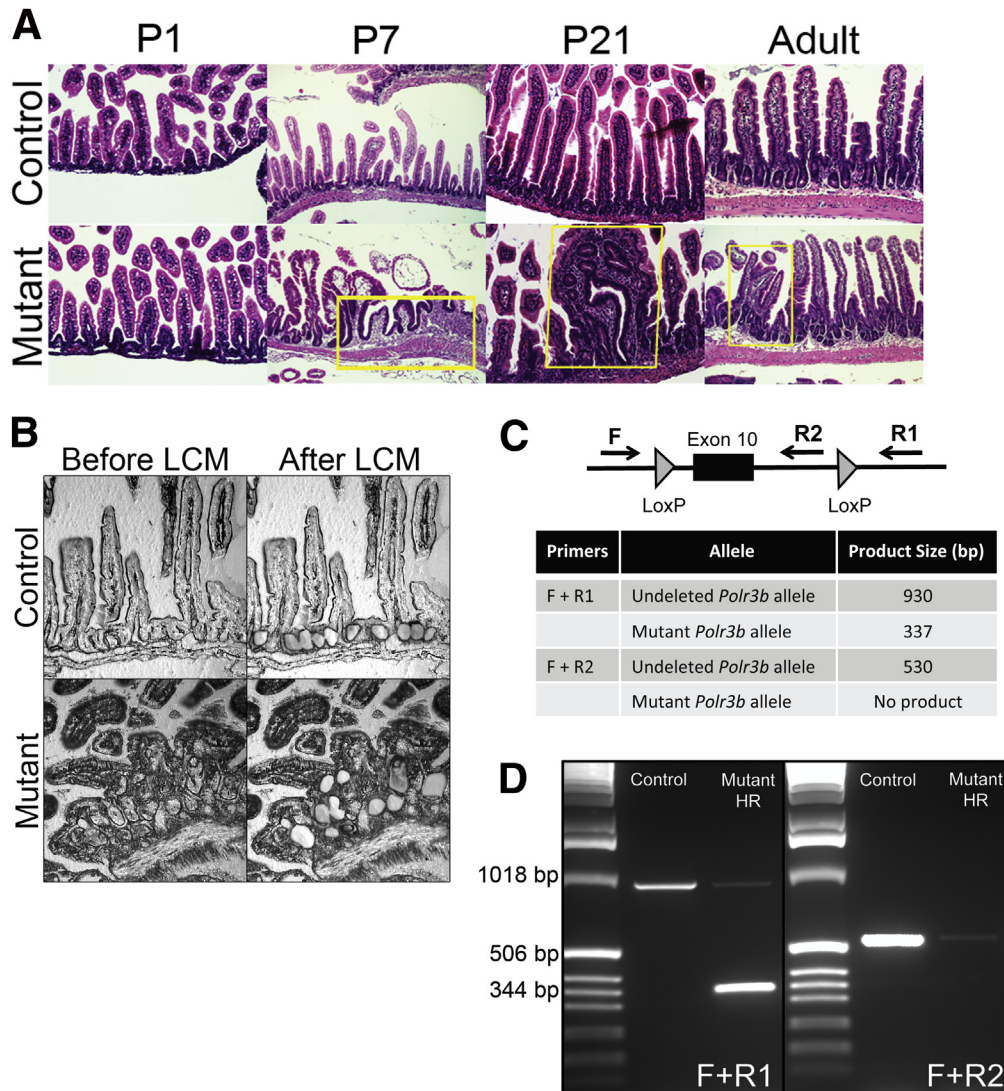


Figure 3. Hyperplastic regions of the *Polr3b*-mutant intestinal epithelium at P21 contain wild-type Cre-escaper cells with the undeleted *Polr3b* allele. (A) H&E staining of the intestinal epithelium showing the morphology of the jejunal epithelium of control and mutant mice at P1 (magnification, 20 \times), P7 (magnification, 10 \times), P21 (magnification, 20 \times), and in adults (age, 2–3 mo) (magnification, 20 \times). Areas with expanded mesenchyme, villus branching, and lack of developing crypts are present in P7 *Polr3b*-mutant epithelium (yellow box). At P21, hyperplastic areas are clearly visible in mutant mice (yellow box). In adults, the intestinal epithelium of *Polr3b*-mutant mice shows improved morphology; however, areas with villus branching still are detected (yellow box). (B) Representative pictures before and after laser capture microdissection (LCM) of crypts dissected from 3-week-old control mice and hyperplastic regions from mutant mice. (C) Scheme of primer design and PCR product size for amplification using different primer sets for LCM-PCR analysis. Primers F and R1 were designed surrounding the loxP sites flanking exon 10 of the *Polr3b* gene, resulting in the amplification of the longer, undeleted *Polr3b* PCR product (1018 bp) or the shorter, mutant *Polr3b* gene PCR product (337 bp). An additional reverse primer (R2) was designed within the loxP-flanked region of the *Polr3b* gene, which when used with the forward (F) primer, results in the amplification of the undeleted *Polr3b* PCR product only (530 bp). (D) PCR results for LCM-dissected regions from control crypts (control) and *Polr3b*-mutant crypts from hyperplastic regions (mutant HR), showing the presence of the undeleted *Polr3b* allele in control crypts, and both deleted as well as undeleted alleles in *Polr3b*-mutant crypts from hyperplastic regions using both primer combinations (F + R1 and F + R2).

Mutant Mice Develop Abnormal Intestinal Epithelial Architecture

Morphologically, the intestinal epithelium of young *Polr3b*-mutant mice was affected severely, showing abnormal crypt and villus architecture (Figure 3A). At earlier developmental stages (E17.5 and P1), no obvious morphologic defects were detected in mutants (data not

shown and Figure 3A, respectively). By P7, epithelial defects were present in all regions of the mutant small intestine and were characterized by an expanded mesenchymal layer, lack of developing crypts, and branched villus-like structures (Figure 3A). At weaning (P21), the intestinal epithelium of *Polr3b*-mutant mice continued to show similar morphologic changes to those seen at P7. In

addition, the P21 epithelium contained areas with dramatic hyperplasia (Figure 3A). In contrast to younger animals, a large fraction of the epithelium of adult mutant mice had normal morphology. However, regions of disorganized epithelium with branched villi and crypt expansion still were detected in adult *Polr3b*-mutants (Figure 3A).

Undeleted Cre Escaper Cells Proliferate in Hyperplastic Regions of Mutant Intestinal Epithelium

The regenerative response, indicated by the presence of hyperplastic regions and increased proliferation of the intestinal epithelium seen in P21 *Polr3b*-mutant mice (Figure 3A), could be explained by stem cells that had escaped Cre-mediated gene ablation. Such incomplete gene deletion has been reported previously in other studies using the Cre system in the mouse intestinal epithelium.²⁴ Epithelial stem and transit-amplifying cells that escape Cre-mediated mutation, and thus have retained normal *Polr3b* function, would be expected to have a significant growth advantage over mutant cells.

To assess the presence of undeleted Cre escaper cells in *Polr3b*-mutant mice in vivo, we performed laser capture microdissection to dissect crypts from control mice and from hyperplastic regions in *Polr3b*-mutant mice (Figure 3B). Subsequently, we PCR-amplified the region of the *Polr3b* locus encoding the loxP sites to detect undeleted and deleted *Polr3b*-mutant alleles. Indeed, the presence of the undeleted *Polr3b* allele in the hyperplastic areas of the intestinal epithelium of *Polr3b^{loxP/loxP};VillinCre* mice was confirmed by PCR assay using 2 sets of primers (Figure 3C and D). These data indicate the presence of wild-type escaper cells with the undeleted allele in the *Polr3b*-mutant intestinal epithelium, which likely were driving the regenerative response described earlier.

To determine the contribution of apoptosis to the loss of developing crypts in the *Polr3b*-mutant intestinal epithelium, we performed TUNEL assays on P3 (Figure 4A and B) and P21 (Figure 4C and D) intestines. Because of the mosaicism in Cre activity observed in the mutant mouse, to distinguish between escaper regions and recombined (mutant) regions in the epithelium, we crossed our *Polr3b^{loxP/loxP};VillinCre* mice with *R26-stop-EYFP* mice. Thus, in regions where Cre was efficient, the epithelium expressed EYFP as detected by immunostaining (Figure 4A and B). In the control epithelium at P3, no apoptotic cells were detected (Figure 4A), while in the mutant epithelium, apoptotic cells were present in EYFP-positive crypts, but not in EYFP-negative cells (Figure 4B). At P21, apoptotic cells were detected in the mesenchyme, but not the epithelium, of control mice (Figure 4C), but apoptotic crypts with TUNEL-positive cells were detected in the mutant epithelium (Figure 4D). A blinded count of the TUNEL-positive cells per crypt in P21 intestine showed that there were significantly more apoptotic cells in the mutant intestinal epithelium than in the control epithelium (control, 0.2 TUNEL-positive

cells/crypt, $N = 4$; mutant, 1.2 TUNEL-positive cells/crypt, $N = 4$; $P = .0012$) (Figure 4E).

Undeleted Cre Escaper Cell Populations Expand Over Time In Vitro

We hypothesized that if stem cells had escaped Cre-mediated gene ablation, a progressive increase would result in the proportion of cells carrying the undeleted allele as the epithelium expands during development. Therefore, to directly measure changes in the abundance of epithelial cells expressing undeleted *Polr3b^{loxP/loxP}* over time, and without the potential contamination of mesenchymal cells, we harvested epithelial tissue from newborn control and *Polr3b*-mutant mice and cultured it in vitro into enteroids (Figure 5; experimental scheme shown in Figure 5A). Indeed, the fraction of the undeleted allele increased significantly between days 2 and 6 in culture ($P < .05$), initially comprising 18% on day 2 in culture, and increasing to 46% on day 6, as shown by qPCR-based quantification of the undeleted allele shown in Figure 5B.

To determine whether the defects in proliferation observed in vivo in mutant epithelium persisted when the epithelium was cultured in vitro, we immunostained enteroids for Ki67. Although all of the control enteroids formed Ki67-positive crypt-like domains (Figure 5C), indicating the presence of stem cells and transit-amplifying cells, mutant enteroids developed into 2 distinctly different structures: enteroids that resembled controls (Figure 5D), and enteroids that formed dilated, cyst-like structures (Figure 5E). Although the cyst-like enteroids expressed Ki67, they failed to form crypt-like domains.

To assess cell death in vitro, after 6 days in culture we stained enteroids for activated caspase-3 (Figure 5F and G). Control enteroids showed no apoptotic cells within the epithelial layer, caspase-3 staining was present only in dead cells shed into the enteroid lumen (Figure 5F). In contrast, as we also observed by TUNEL staining in vivo, *Polr3b*-deficient enteroids showed a high frequency of apoptotic cells within the enteroid epithelium itself (Figure 5G). This is consistent with the hypothesis that the intestinal epithelium is being repopulated by cells expressing the undeleted allele in response to the increased rate of apoptosis in mutant cells.

Over Time, *Polr3b^{loxP/loxP};VillinCre* Crypts Are Replaced by Highly Proliferative Cre-Escaper Cells In Vivo

To confirm that the regions of disrupted proliferation observed in *Polr3b*-mutant intestine were in tissue where Cre was active, while regions of hyperproliferation were derived from Cre-escapers, we performed Ki67 immunostaining on epithelia from *Rosa26-lox-stop-lox-EYFP;VillinCre* (control) and *Polr3b^{loxP/loxP};Rosa26-lox-stop-lox-EYFP;VillinCre* (mutant) P3 mice (described earlier). As expected, controls uniformly expressed Ki67 at the base of each intervillus region (Figure 6C). In contrast, in regions of mutant epithelium where Cre was active, as indicated by

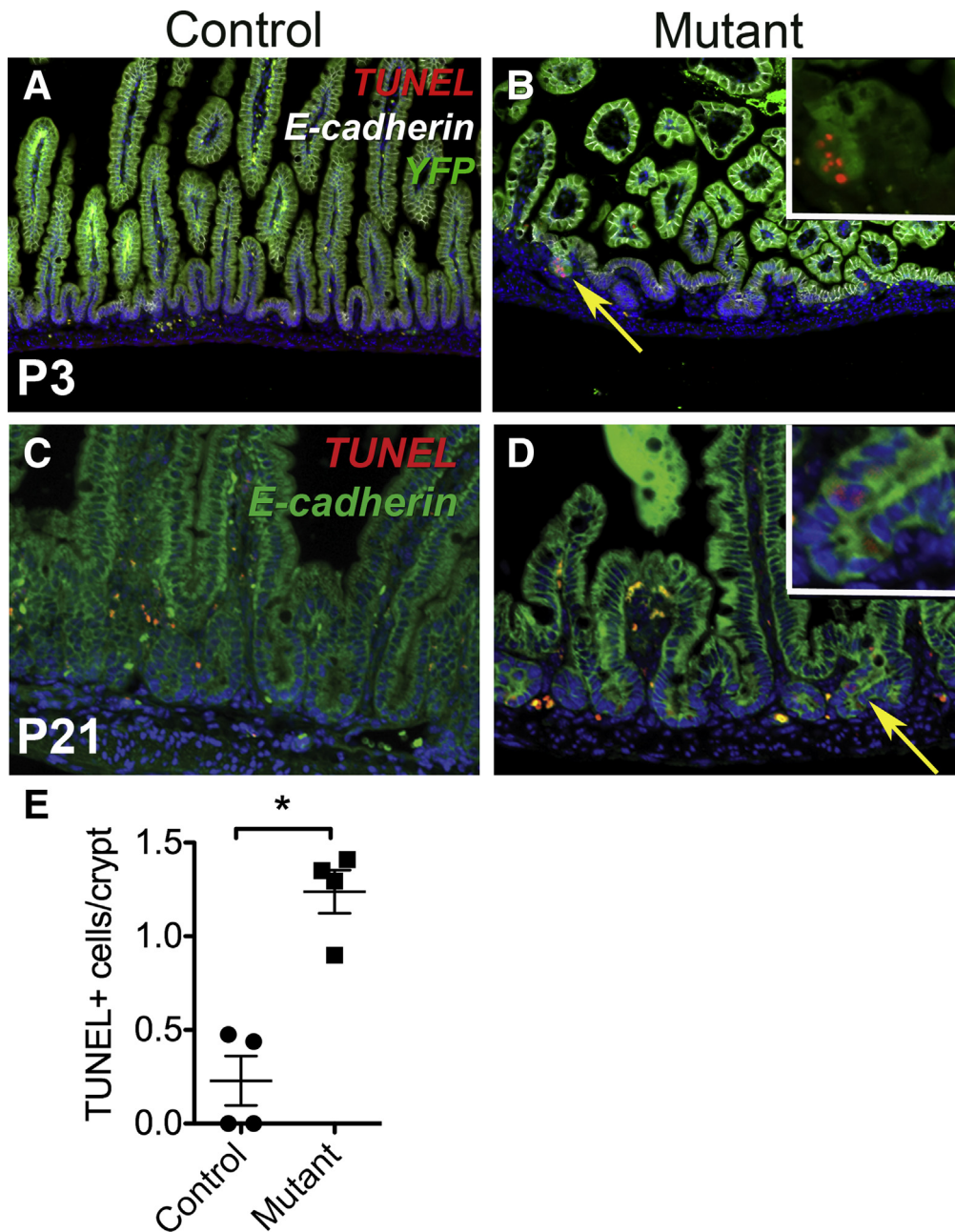


Figure 4. The *Polr3b* mutation is associated with crypt cell death. Apoptotic cells (red) in the crypts were detected by performing the TUNEL assay on intestinal epithelial tissue at (A and B) P3 and (C and D) P21 (weaning). (A and B) Green staining represents EYFP in *Polr3b*^{LoxP/LoxP}; *Rosa26-lox-stop-lox-EYFP*; *VillinCre* mutant or *Rosa26-lox-stop-lox-EYFP*; *Villin-Cre* control mice and is visible only in Cre-expressing tissue. Red, TUNEL; white, E-cadherin; and blue, 4',6-diamidino-2-phenylindole. For increased clarity, the inset in panel B, which is a 3× enlargement of the dying crypt indicated by the yellow arrow, shows only EYFP and TUNEL staining. (C and D) Green, E-cadherin; red, TUNEL; and blue, DAPI. Even during weaning (P21), (C) TUNEL-positive crypts were absent from the control epithelium, (D) but still present in the intestinal epithelium of mutant animals. The inset in D is a 2× enlargement of the dying crypt indicated by the yellow arrow. (A and C) No TUNEL-positive cells were detected in crypts of control mice, although apoptotic cells were detected in the mesenchyme. (B and D) Crypt epithelial cells positive for TUNEL staining were present in *Polr3b*-mutant intestinal epithelium in neonates and during weaning. (B) TUNEL-positive epithelial cells were present only in the tissue where Cre was active in mutant animals. (E) Apoptosis was increased significantly in mutant epithelium at P21. Cell death was quantified by counting the number of TUNEL-positive cells per crypt in jejunal sections from P21 mice (control, N = 4; mutant, N = 4; *P < .002, Student t test).

EYFP staining, very little Ki67 was detected, whereas in EYFP-negative Cre-escaper regions, intervillus regions were expanded and contained dense clusters of Ki67-positive cells (Figure 6D, yellow bracket).

The nonproliferative, Ki67-negative regions interspersed with hyperproliferative crypts observed in the *Polr3b*-mutant small intestine resemble small intestinal epithelium that regenerates after exposure to ionizing radiation. The

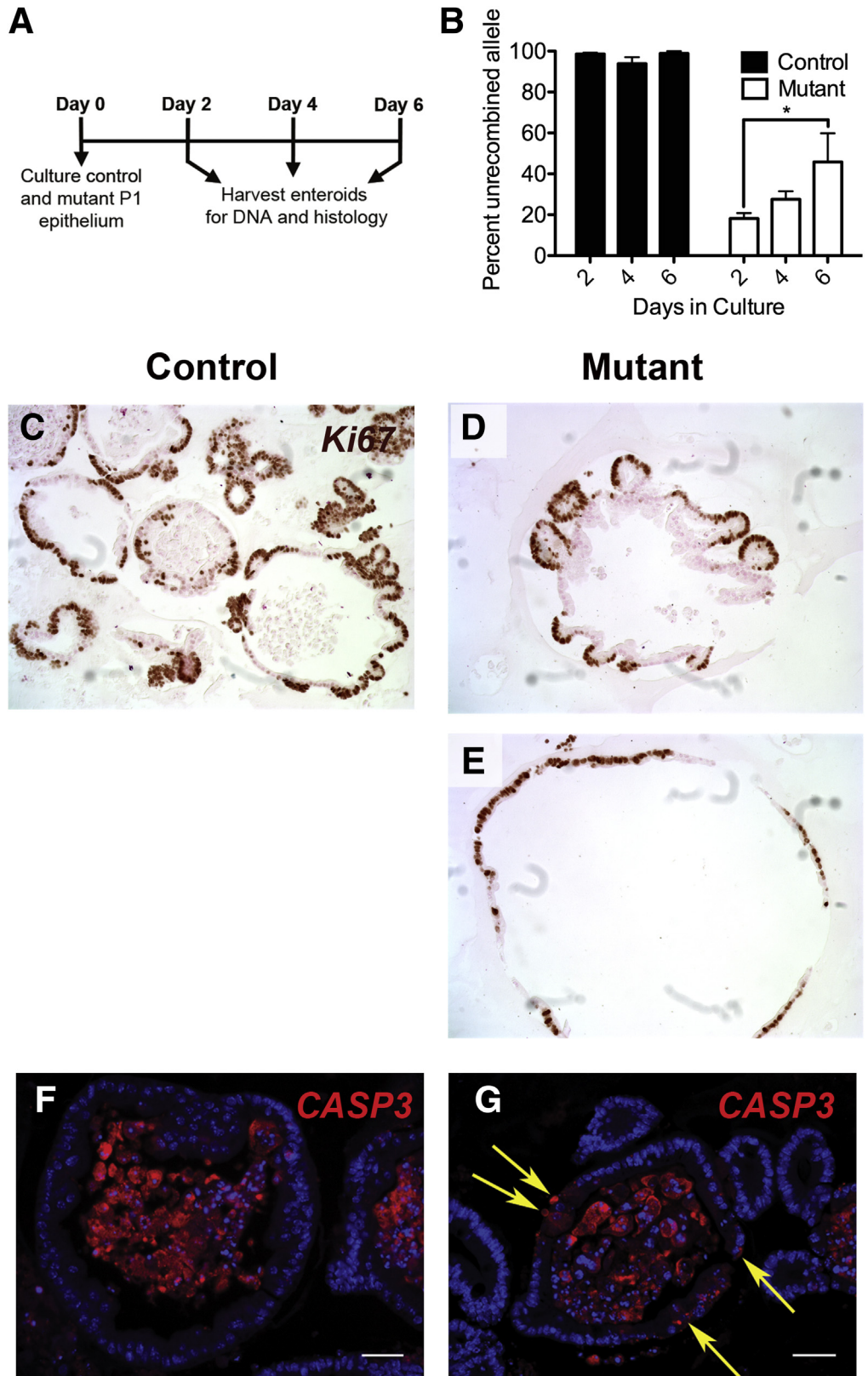
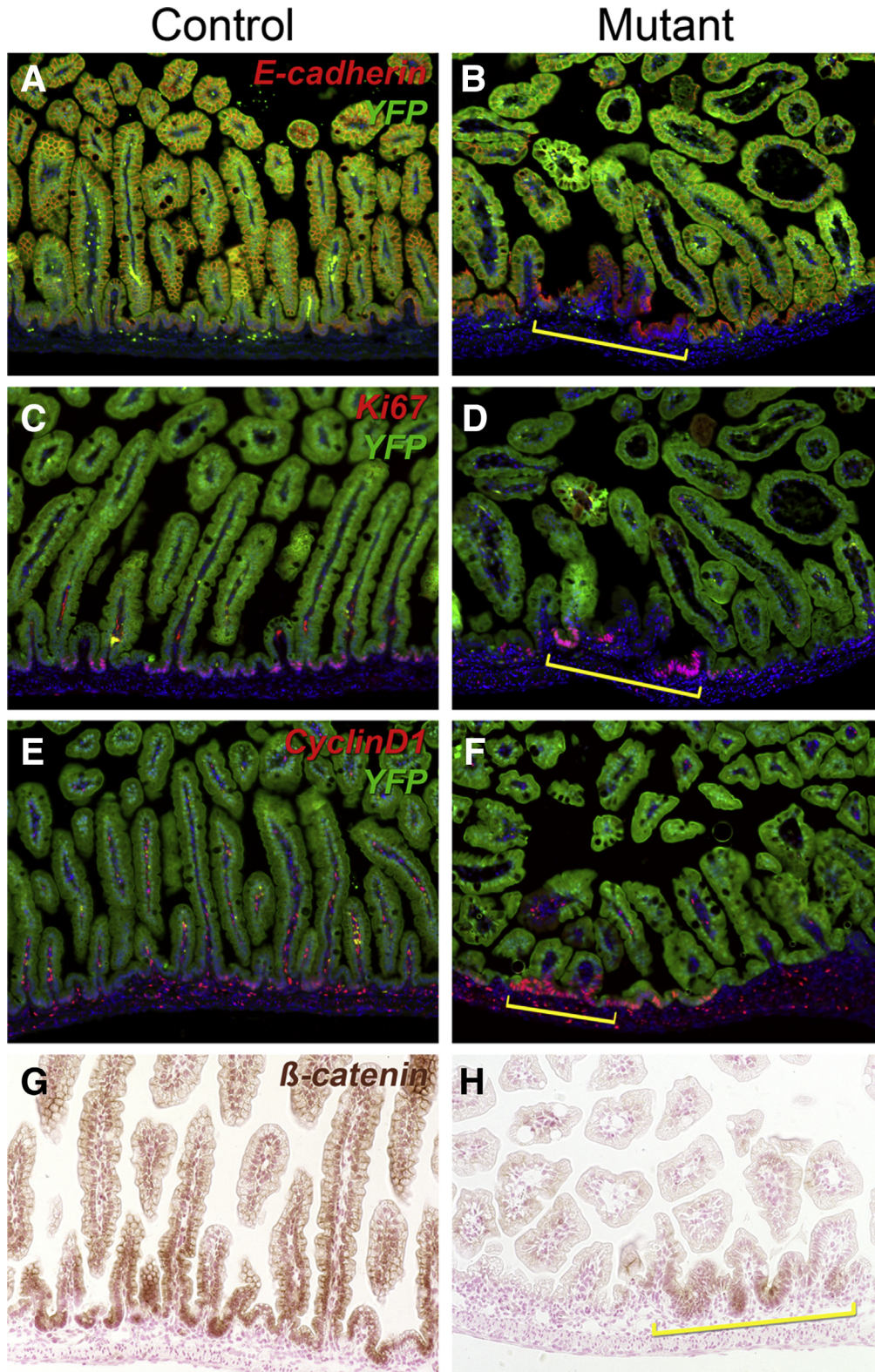


Figure 5. Increased cell death was accompanied by expansion of Cre-escaper cells in the *Polr3b* mutant epithelium in vitro. (A) Scheme for the culture and harvesting of P1 intestinal enteroids. (B) Quantification of the undeleted *Polr3b* exon 10 in genomic DNA from enteroids after 2, 4, and 6 days in culture, as shown in panel E (control, N = 5; mutants, N = 6; error bars indicate SEM; * $P < .05$, Kruskal-Wallis test of mutants followed by the Dunn multiple comparison test). (C–E) Ki67 staining of enteroids from P1 gut after 4 days in culture. Mutant enteroids developed into 2 distinctly different structures: (D) enteroids with Ki67 expression at the tips of crypt-like buds, (C) resembling controls, and (E) dilated, cyst-like structures with patches of Ki67 expression surrounded by flattened Ki67-negative cells. (F and G) Cleaved caspase 3 (CASP3; red) staining of enteroids from P1 gut after 6 days in culture (blue, 4',6-diamidino-2-phenylindole). Increased cell death was detected in *Polr3b*-mutant enteroids compared with controls. (F) In control enteroids, cell death was detected only in cells shed into the lumen, whereas (G) in mutant enteroids, cell death also was seen in peripheral cells that formed the actual enteroid (yellow arrows). Magnification, $\times 40$. Scale bar: 50 $\mu\text{mol/L}$.

regenerative response in injured intestine is driven by Wnt signaling.²⁶ Indeed, even in irradiated crypts in which *Lgr5*⁺ stem cells have been ablated, constitutive activation of Wnt by ablation of *Apc* is sufficient to drive crypt hyperplasia.²⁷

Therefore, to determine whether Wnt pathway activation contributed to proliferation in escaper regions of *Polr3b*-deficient gut, we performed immunostaining for the Wnt target cyclin D1.



At P3, immunohistochemical staining showed that in controls, cyclin D1 was expressed uniformly in the intervillus regions (Figure 6E), whereas mutant regions (EYFP-positive regions) of the *Polr3b*-mutant epithelium lacked cyclin D1-positive cells (Figure 6F). In contrast, EYFP-negative regions of the P3 *Polr3b*-mutant epithelium (highlighted by a yellow bracket), showed dense clusters of cyclin D1-positive cells (Figure 6F). Lack of active Wnt signaling in the *Polr3b*-deficient small intestine was confirmed by staining for β -catenin. As shown in Figure 6G, in control tissue, intervillus regions show strong cytoplasmic and nuclear β -catenin staining, indicative of Wnt pathway activation. In striking contrast, most of the P3 *Polr3b*-mutant epithelium is β -catenin negative, with the exception of an area of regenerative epithelium bracketed in yellow (Figure 6H).

Discussion

Previous studies in yeast and zebrafish have shown the importance of the RNA Pol III complex in cell growth and tissue development. More specifically, the zebrafish mutant *slj*, with a mutation in the second largest Pol III subunit *Polr3b*, causes defects in digestive tract development.¹⁶ Here, we present a model to study the role of Pol III in mammalian intestinal epithelial development and proliferation. We show that decreased activity of the Pol III complex in the mouse intestinal epithelium leads to increased mortality of *Polr3b*-mutant mice in the first postnatal week. Surviving *Polr3b*-mutant mice show reduced proliferation, impaired crypt development, and loss of active Wnt signaling. This initial phenotype is followed by a regenerative response around weaning, which is driven by cells that escape Cre-mediated mutation (Figure 7A). Because of the diminished Pol III activity caused by the *Polr3b* mutation, and resulting low levels of 5S rRNA and U6 snRNA, the high demand for protein synthesis during early intestinal epithelial tissue expansion cannot be met. These events result in impaired crypt development and increased apoptosis in crypts. These data show the important role of *Polr3b* and the Pol III complex in the establishment of the intestinal epithelium during early postnatal life in mammals (Figure 7B). The conditional hypomorphic *Polr3b*-mutant mice described earlier will allow a detailed investigation

of the contribution of RNA polymerase III in all tissue and cell types for which a Cre line is available.

The epithelium of the small intestine is the most rapidly self-renewing mammalian tissue, and thus it is required to be capable of modulating protein synthesis in response to environmental stress or during tissue expansion/growth. During periods of starvation, the gut responds by decreasing villus size, crypt size, and the rate of cell cycling.²⁸ Protein malnutrition alone also results in histologic abnormalities, such as villi fused at the base accompanied by villus blunting, or even the absence of villus architecture.²⁹ The Pol III complex plays an essential role in protein synthesis in all eukaryotic cells.³⁰ Therefore, sufficient Pol III activity is predicted to be essential for intestinal epithelial function and survival.

The simplest explanation of the disrupted development of the small intestine of *Polr3b* mutants is that the reduced Pol III activity impairs cell proliferation because the high metabolic demands of the epithelium cannot be met. Indeed, the mutant intestine shows several similarities to both fasted and protein-starved small intestines: a decrease in cycling cells, abnormal branched villus architecture, and increased apoptosis in epithelial cells.^{28–31} The *Polr3b* mutant intestine thus mimics the malnourished state because the levels of 5S rRNA and U6 snRNA, which are required for protein synthesis, are decreased as a result of low Pol III activity. Defects in protein production machinery thus have a phenotype reminiscent of amino acid deficiency, because in both cases the high demand for protein synthesis during early intestinal epithelial tissue expansion cannot be met.

Yeast and zebrafish studies have suggested that the structural effects of *Polr3b* mutations resulting in impaired transcription by Pol III are caused by the destabilization of the interaction between the *Polr3b* protein and another Pol III subunit, *Polr3k*.^{16,32} The yeast homolog of *Polr3k* is required for Pol III to efficiently perform multiple rounds of transcription on the same gene, which determines the overall output of the complex.³³ Thus, the *Polr3b* mutation in mice results in a reduction in the overall abundance of Pol III transcripts, but without a complete loss of transcription by Pol III, as also was evident by the reduction, but not elimination, of Pol III transcripts in the mutant intestine we documented in Figure 1.

Figure 6. (See previous page). Hyperproliferative Cre-escaper cells repopulate the *Polr3b*-mutant intestinal epithelium. *Rosa26-lox-stop-lox-YFP* mice were crossed with *Polr3b*^{LoxP/LoxP}; *VillinCre* mice to show which sections of the tissue are *Polr3b* mutant (YFP-positive), and which are *Polr3b* wild-type Cre-escaper cells (YFP-negative). (A and B) Red, E-cadherin; green, EYFP; and blue, 4',6-diamidino-2-phenylindole. (A) *Rosa26-lox-stop-lox-YFP*; *VillinCre* (control) jejunum. (B) *Polr3b*^{LoxP/LoxP}; *Rosa26-lox-stop-lox-YFP*; *VillinCre* (mutant) jejunum. The yellow bracket indicates a Cre-escaper region that is negative for YFP. (C and D) Red, Ki67; green, EYFP; and blue, 4',6-diamidino-2-phenylindole. (D) Crypts in the Cre-escaper region (yellow bracket) of the mutant intestine have (C) a higher density of Ki67-positive cells than crypts in the control intestine. (D) Almost no Ki67 was visible in *Polr3b* mutant tissue outside the bracketed area. (E and F) Red, cyclin D1; green, EYFP; and blue, 4',6-diamidino-2-phenylindole. (F) In *Polr3b*-mutant mice, expression of the Wnt target protein cyclin D1 is reduced in mutant tissue compared with the (E) control intestine, whereas escaper regions have dramatically increased cyclin D1 staining (yellow bracket). (G and H) Brown, β -catenin; red, nuclear fast red counterstain. (G) *Rosa26-lox-stop-lox-YFP*; *VillinCre* (control) jejunum. (H) *Polr3b*^{LoxP/LoxP}; *Rosa26-lox-stop-lox-YFP*; *VillinCre* (mutant) jejunum. The yellow bracket indicates a Cre-escaper region that has active Wnt signaling, as indicated by nuclear β -catenin staining.

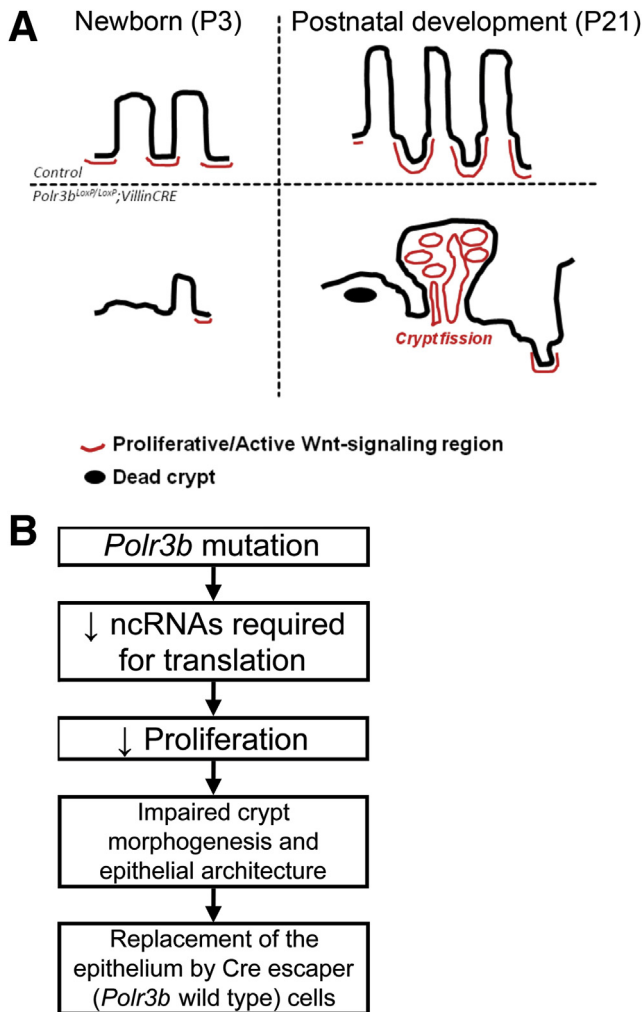


Figure 7. Summary of the effects of the hypomorphic *Polr3b* mutation on the intestinal epithelium. (A) Shortly after birth, large areas lacking proliferative capacity are present in mutant mice (newborn [P3]). During weaning (P21), regions with abnormal crypt architecture lacking proliferative capacity still are present. By P21, hyperplastic regions, which are initiated by the wild-type stem cells that have escaped Cre recombination of the *Polr3b* gene, are evident. These regions repopulate the intestinal epithelium, resulting in normalization of epithelial morphology in *Polr3b*-mutant intestinal epithelium in adults. (B) The mutation in *Polr3b* leads to reduced Pol III activity, which causes impaired transcription of small noncoding RNAs required for translation, resulting in increased crypt cell death, decreased proliferative activity, impaired crypt maturation, and altered epithelial architecture in mutant tissue. The increased death of mutant cells creates a selective advantage for Cre-escaper cells in the intestinal epithelium of *Polr3b*-mutant mice.

Not surprisingly, rapidly dividing cancer cells have an extremely high demand for protein synthesis, and tRNA abundance is increased in many cancers such as multiple myeloma and breast cancer.^{9,34} Multiple oncogenic (extracellular signal-regulated kinase (ERK), TORC1, and MYC) and tumor suppressor (p53, MAF1, retinoblastoma)

pathways regulate RNA polymerase III activity and thus tRNA abundance (reviewed by White² and Grewal⁷). Given the development of small-molecule inhibitors of RNA polymerase III, reducing tRNA abundance has been suggested as a novel targeted approach for cancer therapy. Indeed, in a recent report, Yee et al¹⁶ used the RNA polymerase III inhibitor ML-60218 developed by Wu et al³⁵ in combination with the histone deacetylase inhibitor suberoylanilide hydroxamic acid to reduce proliferation in 2 human pancreatic adenocarcinoma cell lines.³⁶ As noted by the investigators, the safety of ML-60218 in human beings has not yet been evaluated. Given the striking dependency of the mammalian intestinal epithelium on normal rates of RNA polymerase III we showed earlier, it is questionable if globally acting, small-molecule inhibitors of this enzyme can be developed into successful drugs to treat cancer.

References

- de Santa Barbara P, van den Brink GR, Roberts DJ. Development and differentiation of the intestinal epithelium. *Cell Mol Life Sci* 2003;60:1322–1332.
- White RJ. RNA polymerases I and III, non-coding RNAs and cancer. *Trends Genet* 2008;24:622–629.
- Dumay-Odelot H, Durrieu-Gaillard S, Da Silva D, et al. Cell growth- and differentiation-dependent regulation of RNA polymerase III transcription. *Cell Cycle* 2010;9:3687–3699.
- Roberts DN, Stewart AJ, Huff JT, et al. The RNA polymerase III transcriptome revealed by genome-wide localization and activity-occupancy relationships. *Proc Natl Acad Sci U S A* 2003;100:14695–14700.
- Orioli A, Praz V, Lhote P, et al. Human MAF1 targets and represses active RNA polymerase III genes by preventing recruitment rather than inducing long-term transcriptional arrest. *Genome Res* 2016;26:624–635.
- White RJ. Transcription by RNA polymerase III: more complex than we thought. *Nat Rev Genet* 2011;12:459–463.
- Grewal SS. Why should cancer biologists care about tRNAs? tRNA synthesis, mRNA translation and the control of growth. *Biochim Biophys Acta Gene Regul Mech* 2014;1849:898–907.
- Winter AG, Sourvinos G, Allison SJ, et al. RNA polymerase III transcription factor TFIIC2 is overexpressed in ovarian tumors. *Proc Natl Acad Sci U S A* 2000;97:12619–12624.
- Pavon-Eternod M, Gomes S, Geslain R, et al. tRNA overexpression in breast cancer and functional consequences. *Nucleic Acids Res* 2009;37:7268–7280.
- Chen W, Bocker W, Brosius J, et al. Expression of neural BC200 RNA in human tumours. *J Pathol* 1997;183:345–351.
- Singh K, Carey M, Saragosti S, et al. Expression of enhanced levels of small RNA polymerase III transcripts encoded by the B2 repeats in simian virus 40-transformed mouse cells. *Nature* 1985;314:553–556.
- Gomez-Roman N, Grandori C, Eisenman R, et al. Direct activation of RNA polymerase III transcription by c-Myc. *Nature* 2003;421:290–294.

13. Chesnokov I, Chu WM, Botchan MR, et al. p53 inhibits RNA polymerase III-directed transcription in a promoter-dependent manner. *Mol Cell Biol* 1996;16:7084–7088.
14. White RJ, Trouche D, Martin K, et al. Repression of RNA polymerase III transcription by the retinoblastoma protein. *Nature* 1996;382:88–90.
15. Michels AA, Robitaille AM, Buczynski-Ruchonnet D, et al. mTORC1 directly phosphorylates and regulates human MAF1. *Mol Cell Biol* 2010;30:3749–3757.
16. Yee NS, Gong W, Huang Y, et al. Mutation of RNA Pol III subunit *rpc2/polr3b* leads to deficiency of subunit *Rpc11* and disrupts zebrafish digestive development. *PLoS Biol* 2007;5:2484–2492.
17. Rodríguez CI, Buchholz F, Galloway J, et al. High-efficiency deleter mice show that *FLPe* is an alternative to *Cre-loxP*. *Nat Genet* 2000;25:139–140.
18. Madison BB, Dunbar L, Qiao XT, et al. *cis* elements of the villin gene control expression in restricted domains of the vertical (crypt) and horizontal (duodenum, cecum) axes of the intestine. *J Biol Chem* 2002;277:33275–33283.
19. Gao N, White P, Doliba N, et al. *Foxa2* controls vesicle docking and insulin secretion in mature beta cells. *Cell Metab* 2007;6:267–279.
20. Salzman NH, Hung K, Haribhai D, et al. Enteric defensins are essential regulators of intestinal microbial ecology. *Nat Immunol* 2010;11:76–83.
21. Foureau DM, Mielcarz DW, Menard LC, et al. TLR9-dependent induction of intestinal alpha-defensins by *Toxoplasma gondii*. *J Immunol* 2010;184:7022–7029.
22. Inoue R, Tsuruta T, Nojima I, et al. Postnatal changes in the expression of genes for cryptdins 1–6 and the role of luminal bacteria in cryptdin gene expression in mouse small intestine. *FEMS Immunol Med Microbiol* 2008;52:407–416.
23. Sakamori R, Das S, Yu S, et al. *Cdc42* and *Rab8a* are critical for intestinal stem cell division, survival, and differentiation in mice. *J Clin Invest* 2012;122:1052–1065.
24. de Lau W, Barker N, Low TY, et al. *Lgr5* homologues associate with Wnt receptors and mediate R-spondin signalling. *Nature* 2011;476:293–297.
25. Sato T, Vries RG, Snippert HJ, et al. Single *Lgr5* stem cells build crypt-villus structures in vitro without a mesenchymal niche. *Nature* 2009;459:262–265.
26. Clevers H, Loh KM, Nusse R. Stem cell signaling. An integral program for tissue renewal and regeneration: Wnt signaling and stem cell control. *Science* 2014;346:1248012.
27. Metcalfe C, Kljavin NM, Ybarra R, et al. *Lgr5+* stem cells are indispensable for radiation-induced intestinal regeneration. *Cell Stem Cell* 2014;14:149–159.
28. Altmann GG. Influence of starvation and refeeding on mucosal size and epithelial renewal in the rat small intestine. *Am J Anat* 1972;133:391–400.
29. Tandon BM, Magotra ML, Saraya AK, et al. Small intestine in protein malnutrition. *Am J Clin Nutr* 1968;21:813–819.
30. White RJ. RNA polymerase III transcription and cancer. *Oncogene* 2004;23:3208–3216.
31. Boza JJ, Moennoz D, Vuichoud J, et al. Food deprivation and refeeding influence growth, nutrient retention and functional recovery of rats. *J Nutr* 1999;129:1340–1346.
32. Landrieux E, Alic N, Ducrot C, et al. A subcomplex of RNA polymerase III subunits involved in transcription termination and reinitiation. *EMBO J* 2006;25:118–128.
33. Flores A, Briand JF, Gadal O, et al. A protein-protein interaction map of yeast RNA polymerase III. *Proc Natl Acad Sci U S A* 1999;96:7815–7820.
34. Zhou Y, Goodenbour JM, Godley LA, et al. High levels of tRNA abundance and alteration of tRNA charging by bortezomib in multiple myeloma. *Biochem Biophys Res Commun* 2009;385:160–164.
35. Wu L, Pan J, Thoroddsen V, et al. Novel small-molecule inhibitors of RNA polymerase III. *Eukaryot Cell* 2003;2:256–264.
36. Yee NS, Zhou W, Chun SG, et al. Targeting developmental regulators of zebrafish exocrine pancreas as a therapeutic approach in human pancreatic cancer. *Biol Open* 2012;1:295–307.

Received August 24, 2014. Accepted August 17, 2016.

Correspondence

Address correspondence to: Klaus H. Kaestner, PhD, 12-126 Smilow Center for Translational Research, University of Pennsylvania, Perelman School of Medicine, 3400 Civic Center Boulevard, Philadelphia, Pennsylvania 19104. e-mail: kaestner@mail.med.upenn.edu; fax: (215) 573-5892; or Michael Pack, MD, University of Pennsylvania, Perelman School of Medicine, 1212 Biomedical Research Building II/III, 421 Curie Boulevard, Philadelphia, Pennsylvania 19104. e-mail: mpack@mail.med.upenn.edu; fax: (215) 898-9871.

Acknowledgments

The authors thank Karrie Brondell and Tia Bernard-Banks for maintenance of the mouse colony, and Shiqi Ma, Wen Lin, and Amber Riblett for excellent technical assistance. The authors thank Drs Nuria Brämswig, Karyn Sheaffer, and Logan Everett for helpful suggestions and discussions.

Conflicts of interest

The authors disclose no conflicts.

Funding

Supported by the NIDDK grant R01-DK053839 and the NIDDK grant R37-DK053839 (K.H.K.). Gary Swain and the Morphology Core of the Penn Center for the Study of Digestive and Liver Diseases were supported by P30-DK050306.